This is a repository copy of *Determination of the thermo-physical properties of multi-layered biological tissues*.

White Rose Research Online URL for this paper:
https://eprints.whiterose.ac.uk/175610/

Version: Accepted Version

Determination of the thermo-physical properties of multi-layered biological tissues

M. Alosaimi[1,2], D. Lesnic[1,*] and J. Niesen[1]

[1]*Department of Applied Mathematics, University of Leeds, Leeds LS2 9JT, UK*

[2]*Department of Mathematics and Statistics, College of Science, Taif University, P.O. Box 11099, Taif 21944, Saudi Arabia*

E-mails: mmmaal@leeds.ac.uk (M. Alosaimi), amt5ld@maths.leeds.ac.uk (D. Lesnic* corresponding author), j.niesen@leeds.ac.uk (J. Niesen)

Abstract. Abnormal biological tissues possess unknown properties that must be estimated in order to decide the appropriate method of treatment in terms of amount of dosage and appropriate place of inoculation. The current work numerically investigates, for the first time, the simultaneous estimation of several thermo-physical properties of multi-layered tissues from internal temperature measurements. The heat propagation within the tissues is modelled by the thermal-wave model of bio-heat transfer, accounting for the finite speed of heat propagation. On the skin surface, a convective boundary condition holds taking into account the heat exchange with the environment, whilst on the most inner wall of the tissues a Dirichlet boundary temperature condition is prescribed. Accurate and stable reconstruction of the piecewise constant properties given by the thermal conductivity, heat capacity and blood perfusion rate is successfully achieved for two physical examples concerning three- and four-layered, one-dimensional tissues, subjected to externally induced aggression.

Keywords: Inverse problem; bio-heat transfer; thermal-wave model; stratified tissue.

1. Introduction

Cancer is recognised as the leading cause of death globally, [1]. It has been the focus of extensive research concerning its presence, spread and treatment in the past decades. Determining its early presence and how it might grow can significantly assist in evaluating the efficiency of medical treatments. Many therapeutic procedures such as thermotherapy, cryosurgery and chemotherapy have been utilised to treat cancer. For instance, in hyperthermia treatment, to eradicate tumours, clinical therapists aim to elevate the temperature of the unhealthy tissues to about 42-46 °C, while maintaining the healthy tissues unharmed, [1, 2].

The use of mathematical modelling has been a success in most practical biomedical applications such as identifying the characteristics of tumours, optimising the thermal dose required in cancer treatments or computing the thermal damage caused by medical therapies. In this regard, the parabolic Pennes' bio-heat model [3] has been the most widely used model. In spite of this wide acceptance, the Pennes' bio-heat model breaks down because it assumes that the propagation of heat is infinite. However, as observed experimentally, heat in biological bodies propagates at a finite speed, [4–6]. This realistic feature is accounted for by the thermal-wave model of bio-heat transfer (or sometimes called the single-phase-lag model) developed by Liu et al. [7]. More recently, the dual-phase-lag model has been increasingly used in modelling of bioheat transfer, [8–10]. To mention a few studies, Tunç et al. [1] obtained the temperature profile of a four-layered thigh tissue irradiated by external heating using the Pennes' bio-heat model in order to assist medical practitioners in treating cancer. Based on the Pennes' bio-heat model and an Arrhenius-type integral, Autrique and

Lormel [11] were able to evaluate the thermal damage due to a burn injury.

In most biomedical situations related to biological tissues, parts of the data, such as the thermo-physical properties of the tissues considered, are unknown and cannot be directly measured by experiments, [12]. Nevertheless, inverse analysis has been a useful tool to indirectly estimate such missing input. Research in this direction proceeds by recasting the inverse problem at hand as a constrained non-linear minimisation problem which is solved by invoking an optimisation method such as the golden section search method (GSSM) [13], genetic algorithms [14], or the conjugate gradient method (CGM) [15]. Other important methodologies are based on Bayesian analysis such as the Markov Chain Monte Carlo (MCMC) method [16].

Previous inverse problems in biomedical engineering and medical physics have looked at several applications such as tumour detection, the identification of thermo-physical properties and optimising cancer treatments. To mention a few applications, Panda and Das [13] retrieved the metabolism of both healthy and unhealthy tissues to identify a tumour by utilising the parabolic Pennes' bio-heat model and the GSSM. Similarly, Das and Mishra [14] identified the size, location and properties of a tumour using a genetic algorithm. The identification of tumour size and location on the basis of the knowledge of temperature on the skin surface was investigated in [17] and [18] based on steady-state and transient thermal analysis, respectively. Panda and Das [19] non-intrusively reconstructed the blood perfusion rate in a single-layered tissue from its surface temperature using the thermal-wave model of bio-heat transfer in conjunction with the differential evolution algorithm. Baghban and Ayani [2] estimated the intensity of a laser applied to a three-layered skin tissue using the parabolic Pennes' bio-heat model and a sequential method. Very recently, the retrieval of several thermo-physical properties of a single-layer tissue entering a thermal-wave model of bioheat transfer has been investigated by Alosaimi et al. [20]. These previous studies either neglected the stratified structure of the tissues investigated or did not consider the thermal-wave model of bio-heat transfer. It is the purpose of this work to account for these extra characteristics, in addition to investigating the simultaneous estimation of several thermo-physical properties of multi-layered tissues, as illustrated in Figure 1.
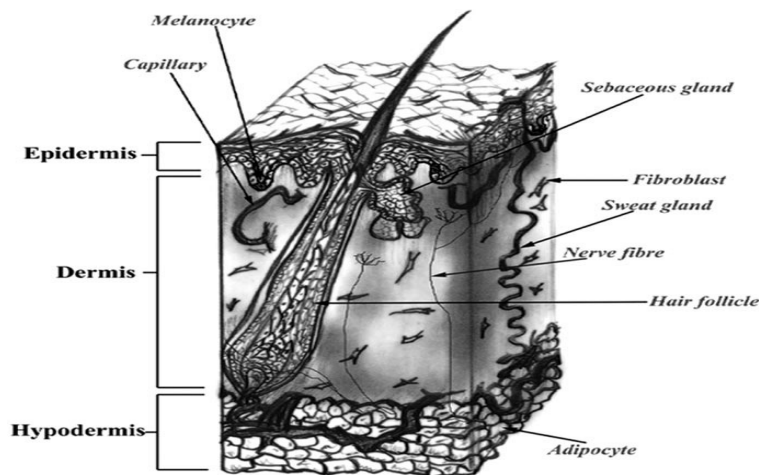

Figure 1: Triple-layered skin tissue, [21].

2

The rest of the paper is organised as follows. In Section 2, the thermal-wave model of bio-heat transfer for multi-layered tissues is formulated. In Section 3, the finite-difference method (FDM) used as a direct solver is developed, then two direct problems concerning three- and four-layered, one-dimensional tissues subjected to externally induced aggression are numerically solved using the proposed direct solver. Section 4 describes the inversion approach subsequently utilised to recover the thermo-physical properties of interest. Results of the inversion of both exact and noisy data are presented and discussed. Conclusions are given in Section 5.

2. Mathematical formulation

The partial differential equation (PDE) governing the heat propagation in biological tissues is described by the thermal-wave model of bio-heat transfer given by, [7],

$$\rho_t c_t \tau \frac{\partial^2 T}{\partial t^2} + (\rho_t c_t + \tau w_b \rho_b c_b)\frac{\partial T}{\partial t} = k\nabla^2 T + w_b \rho_b c_b (T_a - T) + Q_m + Q_e + \tau \frac{\partial}{\partial t}(Q_m + Q_e),$$
$$\text{in } \Omega \times (0, t_f], \quad (1)$$

where Ω represents the tissue domain, $t_f > 0$ denotes the final time of the transient process, T, ρ_t, c_t and k are the temperature [K or °C], density [kg/m³], specific heat [Joule/(kg K) or Joule/(kg °C)] and thermal conductivity [W/(m K) or W/(m °C)] of the tissue, respectively, ρ_b, c_b and w_b stand for the density [kg/m³], specific heat [Joule/(kg K) or Joule/(kg °C)] and perfusion rate [s^{-1}] of the blood, respectively, τ is the relaxation time [s], ∇^2 is the Laplace operator, t is the time [s] and T_a is the (arterial) blood temperature [K or °C]. Q_m and Q_e are the metabolic and external heats [W/m³]. Also, we denote by $\alpha = k/(\rho_t c_t)$ the thermal diffusivity of the tissue [m²/s]. Equation (1) has been derived by modifying the parabolic Pennes' bio-heat reaction-diffusion equation to take into account for the finite speed (equal to $\sqrt{\alpha/\tau}$) of energy propagation present in biological tissues through the non-negligible relaxation time τ in between 15-30 s for biological bodies, [22]. This gives rise to the generalised Fourier's law (or the Maxwell-Cattaneo equation) expressing the heat flux $\mathbf{q}(\mathbf{x}, t)$ as:

$$-k\nabla T(\mathbf{x}, t) = \mathbf{q}(\mathbf{x}, t + \tau) \approx \mathbf{q}(\mathbf{x}, t) + \tau \frac{\partial \mathbf{q}}{\partial t}(\mathbf{x}, t), \quad (\mathbf{x}, t) \in \Omega \times (0, t_f]. \quad (2)$$

It is interesting to note that the zero-flux boundary condition $\mathbf{q}(\mathbf{x}, t) \cdot \boldsymbol{\nu}(\mathbf{x}) = 0$ on $\partial\Omega \times (0, t_f]$, where $\boldsymbol{\nu}$ is the outward unit normal to the boundary $\partial\Omega$, maintains as the zero-Neumann boundary condition $-k\partial_\nu T = 0$, but a non-zero flux prescription does not maintain its usual form in terms of the normal derivative of T, see Yu [23]. On the other hand, the invariance holds for a Robin boundary condition that arises from a generalised Newton's law of the form, see Maurer and Thompson [24],

$$\left(\mathbf{q}(\mathbf{x}, t) + \tau \frac{\partial \mathbf{q}}{\partial t}(\mathbf{x}, t)\right) \cdot \boldsymbol{\nu}(\mathbf{x}) = -h(T_\infty - T(\mathbf{x}, t)), \quad (\mathbf{x}, t) \in \partial\Omega \times (0, t_f], \quad (3)$$

where h is the heat transfer coefficient [W/(m² K) or W/(m² °C)] and T_∞ represents the ambient temperature [K or °C]. The boundary condition (3) models the transfer of heat from the environment into the biological body by taking into account for the time scale of thermal relaxation, [25, 26]. Then, assuming that (2) holds at the boundary we obtain the usual Newton's law boundary condition, see Hennessy et al. [27],

$$k\nabla T \cdot \boldsymbol{\nu} = h(T_\infty - T) \quad \text{on } \partial\Omega \times (0, t_f]. \quad (4)$$

3

Assuming that the tissue Ω is a one-dimensional composite material formed of J disjoint layers $[L_{l-1}, L_l]$ for $l = \overline{1, \mathrm{J}}$, (notation for $l = 1, \ldots, \mathrm{J}$), equation (1) transforms into, [28],

$$C_{\mathrm{t}}^l \tau_l \frac{\partial^2 T_l}{\partial t^2} + \left(C_{\mathrm{t}}^l + \tau_l w_b^l C_b\right) \frac{\partial T_l}{\partial t} = k_l \frac{\partial^2 T_l}{\partial x^2} + w_b^l C_b (T_a - T_l) + Q_m^l + Q_e^l + \tau_l \frac{\partial}{\partial t}(Q_m^l + Q_e^l),$$
$$(x, t) \in [L_{l-1}, L_l] \times (0, t_{\mathrm{f}}], \quad l = \overline{1, \mathrm{J}}, \quad (5)$$

with the corresponding thermo-physical properties annotated by the super/sub-script l for each layer, and $C_{\mathrm{t}}^l = \rho_{\mathrm{t}}^l c_{\mathrm{t}}^l$ [Joule/(m³ K) or Joule/(m³ °C)] and $C_b = \rho_b c_b$ [Joule/(m³ K) or Joule/(m³ °C)] denoting the heat capacity of the tissue layer l and blood, respectively.

The above equations are coupled through the usual continuity of the temperature at the interfaces, namely,

$$T_l(L_l, t) = T_{l+1}(L_l, t), \quad t \in [0, t_{\mathrm{f}}], \quad l = \overline{1, (\mathrm{J} - 1)}, \quad (6)$$

and of the heat flux. This latter condition needs to be considered more carefully since in the case of the Maxwell-Cattaneo equation (1) (or (5)), the heat flux is given by the generalised Fourier's law (2). Then, on imposing the continuity of the heat flux at the interface $q_l(L_l, t) = q_{l+1}(L_l, t)$, we also have that $\frac{\partial q_l}{\partial t}(L_l, t) = \frac{\partial q_{l+1}}{\partial t}(L_l, t)$ and equation (2) implies that:

$$k_l \frac{\partial T_l}{\partial x}(L_l, t) = k_{l+1} \frac{\partial T_{l+1}}{\partial x}(L_l, t), \quad t \in [0, t_{\mathrm{f}}], \quad l = \overline{1, (\mathrm{J} - 1)}, \quad (7)$$

provided that $\tau_l = \tau_{l+1}$ for $l = \overline{1, (\mathrm{J} - 1)}$, i.e. the relaxation time is the constant $\tau > 0$ over each layer, which we shall assume from now on.

For the governing hyperbolic PDE (5), we assume that the initial temperature is uniform and equal to a constant T_0 while the heating process is initiated from rest, in which case the initial conditions are given by:

$$T_l(x, 0) = T_0, \quad \frac{\partial T_l}{\partial t}(x, 0) = 0, \quad x \in [L_{l-1}, L_l], \quad l = \overline{1, \mathrm{J}}. \quad (8)$$

The upstream end of the tissue $x = L_0$ is assumed in contact with the ambient air while the downstream end $x = L_{\mathrm{J}}$ is kept at a fixed temperature equal to the constant T_0, such that the boundary conditions are given by:

$$-k_1 \frac{\partial T_1}{\partial x}(L_0, t) = h\left(T_\infty - T_1(L_0, t)\right), \quad T_{\mathrm{J}}(L_{\mathrm{J}}, t) = T_0, \quad t \in [0, t_{\mathrm{f}}]. \quad (9)$$

The case of an adiabatic zero-flux Neumann condition $\partial_x T_{\mathrm{J}}(L_{\mathrm{J}}, t) = 0$, instead of the Dirichlet condition $T_{\mathrm{J}}(L_{\mathrm{J}}, t) = T_0$ in (9), has been considered elsewhere, [29].

The next subsection presents a dimensionless version of the thermal-wave model (5)-(9).

2.1 Dimensionless model

The thermal-wave model (5)-(9) can be non-dimensionalised using the change of variables:

$$(\bar{x}, \mathrm{L}_l) = \frac{(x, L_l)}{L_{\mathrm{J}}}, \quad \bar{t} = \frac{t}{t_{\mathrm{f}}}, \quad \theta_l = \frac{T_l - T_0}{T_0}, \quad \theta_\infty = \frac{T_\infty - T_0}{T_0}, \quad F^l = \frac{Q_e^l + Q_m^l}{Q_0}, \quad (10)$$

where Q_0 is the maximum value of the heating applied and generated. Then, the dimensionless version of the thermal-wave model (omitting the bars on x and t for clarity) is obtained as:

$$\frac{\partial^2 \theta_l}{\partial t^2} + a_1^l \frac{\partial \theta_l}{\partial t} = a_2^l \frac{\partial^2 \theta_l}{\partial x^2} - a_3^l \left(\theta_l + \frac{T_0 - T_a}{T_0} \right) + a_4^l \left(F^l + \frac{\tau}{t_f} \frac{\partial F^l}{\partial t} \right),$$

$$(x, t) \in [L_{l-1}, L_l] \times (0, 1], \quad l = \overline{1, J}, \tag{11}$$

subject to the initial conditions:

$$\theta_l(x, 0) = 0, \qquad \frac{\partial \theta_l}{\partial t}(x, 0) = 0, \quad x \in [L_{l-1}, L_l], \quad l = \overline{1, J}, \tag{12}$$

the interface conditions:

$$\theta_l(L_l, t) = \theta_{l+1}(L_l, t), \qquad t \in [0, 1], \qquad l = \overline{1, (J-1)},$$

$$a_5^l \frac{\partial \theta_l}{\partial x}(L_l, t) = \frac{\partial \theta_{l+1}}{\partial x}(L_l, t), \qquad t \in [0, 1], \qquad l = \overline{1, (J-1)}, \tag{13}$$

and the mixed boundary conditions:

$$\theta_1(L_0, t) - a_6 \frac{\partial \theta_1}{\partial x}(L_0, t) = \theta_\infty, \qquad \theta_J(1, t) = 0, \quad t \in \big[0, 1\big], \tag{14}$$

where:

$$a_1^l = \frac{t_f}{\tau} + \frac{w_b^l C_b t_f}{C_t^l}, \quad a_2^l = \frac{k_l t_f^2}{\tau C_t^l L_J^2}, \quad a_3^l = \frac{t_f}{\tau} \left(a_1^l - \frac{t_f}{\tau} \right), \quad a_4^l = \frac{Q_0 t_f^2}{\tau T_0 C_t^l}, \quad l = \overline{1, J},$$

$$a_5^l = \frac{a_2^l a_4^{l+1}}{a_4^l a_2^{l+1}}, \quad l = \overline{1, (J-1)}, \quad a_6 = \frac{Q_0 L_J a_2^1}{h T_0 a_4^1}. \tag{15}$$

The inversion of the above algebraic equations is given by:

$$C_t^l = \frac{Q_0 t_f^2}{\tau T_0 a_4^l}, \quad k_l = \frac{\tau C_t^l L_J^2 a_2^l}{t_f^2}, \quad w_b^l = \frac{C_t^l}{C_b t_f} \left(a_1^l - \frac{t_f}{\tau} \right), \quad l = \overline{1, J}. \tag{16}$$

The next section develops an absolutely stable FDM used as a direct solver, after which two direct problems concerning three- and four-layered, one-dimensional tissues are solved.

3. Numerical solution of direct problem

Denoting $Q^l := [L_{l-1}, L_l] \times (0, 1]$ for $l = \overline{1, J}$, we consider the more generic hyperbolic direct problem associated with (11)-(14) given by:

$$\frac{\partial^2 u_l}{\partial t^2}(x, t) + b_l \frac{\partial u_l}{\partial t}(x, t) = c_l \frac{\partial^2 u_l}{\partial x^2}(x, t) - d_l u_l(x, t) + f_l(x, t), \quad (x, t) \in Q^l, \tag{17}$$

where b_l, c_l and d_l are given positive constants, and f_l are given source functions for $l = \overline{1, J}$, subject to the initial conditions:

$$u_l(x, 0) = \phi_l(x), \qquad \frac{\partial u_l}{\partial t}(x, 0) = \psi_l(x), \quad x \in [L_{l-1}, L_l], \tag{18}$$

where $\phi_l(x)$ and $\psi_l(x)$ are prescribed functions for $l = \overline{1, J}$, the interface conditions:

$$u_l(L_l, t) = u_{l+1}(L_l, t), \qquad t \in [0, 1],$$

$$\gamma_l \frac{\partial u_l}{\partial x}(L_l, t) = \frac{\partial u_{l+1}}{\partial x}(L_l, t), \qquad t \in [0, 1], \tag{19}$$

5

where γ_l are prescribed positive constants for $l = \overline{1,(J-1)}$, and the mixed boundary conditions:

$$u_1(L_0,t) + \beta \frac{\partial u_1}{\partial x}(L_0,t) = R(t), \qquad u_J(L_J,t) = 0, \quad t \in [0,1], \tag{20}$$

where $L_J = 1$, $\beta \neq 0$ is a prescribed constant and $R(t)$ is a prescribed function.

As an alternative to the hyperbolic wave-type equation (17), we introduce the intermediate variable v_l, [30], as:

$$v_l(x,t) := \frac{\partial u_l}{\partial t}(x,t) + b_l u_l(x,t), \quad (x,t) \in Q^l, \quad l = \overline{1,J}, \tag{21}$$

such that equation (17) can be written as:

$$\frac{\partial v_l}{\partial t}(x,t) = c_l \frac{\partial^2 u_l}{\partial x^2}(x,t) - d_l u_l(x,t) + f_l(x,t), \quad (x,t) \in Q^l, \quad l = \overline{1,J}. \tag{22}$$

From (18) and (21), we obtain the initial condition:

$$v_l(x,0) = \psi_l(x) + b_l \phi_l(x), \quad x \in [L_{l-1}, L_l], \quad l = \overline{1,J}. \tag{23}$$

We subdivide the domain Q^l into M^l and N uniform meshes $\Delta x_l = (L_l - L_{l-1})/M^l$ and $\Delta t = 1/N$, respectively. We let $P_0 = 0$ and $P_l = \sum_{r=1}^{l} M^r$ for $l = \overline{1,J}$. At the grid node (x_i, t_j), we denote $u_{i,j}^l := u_l(x_i, t_j)$, $v_{i,j}^l := v_l(x_i, t_j)$, $\left(u_{i,j}^l\right)_x := \frac{\partial u_l}{\partial x}(x_i, t_j)$ and $f_{i,j}^l := f_l(x_i, t_j)$, where $x_i = L_{l-1} + (i - P_{l-1})\Delta x_l$, $t_j = j\Delta t$ for $i = \overline{P_{l-1}, P_l}$, $j = \overline{0,N}$.

The FDM discretises (21) and (22) as:

$$\frac{u_{i,j+1}^l - u_{i,j}^l}{\Delta t} = \frac{1}{2}\left(v_{i,j}^l - b_l u_{i,j}^l + v_{i,j+1}^l - b_l u_{i,j+1}^l\right),$$
$$i = \overline{P_{l-1}, P_l}, \quad j = \overline{0,(N-1)}, \quad l = \overline{1,J}, \tag{24}$$

$$\frac{v_{i,j+1}^l - v_{i,j}^l}{\Delta t} = \frac{1}{2}\left(\frac{c_l}{(\Delta x_l)^2}\delta_x^2 u_{i,j}^l - d_l u_{i,j}^l + f_{i,j}^l + \frac{c_l}{(\Delta x_l)^2}\delta_x^2 u_{i,j+1}^l - d_l u_{i,j+1}^l + f_{i,j+1}^l\right),$$
$$i = \overline{(P_{l-1}+1),(P_l-1)}, \quad j = \overline{0,(N-1)}, \quad l = \overline{1,J}, \tag{25}$$

$$\frac{v_{i,j+1}^l - v_{i,j}^l}{\Delta t} = \frac{1}{2}\left(\frac{2c_l}{(\Delta x_l)^2}\tilde{\delta}_x^2 u_{i,j}^l - d_l u_{i,j}^l + f_{i,j}^l + \frac{2c_l}{(\Delta x_l)^2}\tilde{\delta}_x^2 u_{i,j+1}^l - d_l u_{i,j+1}^l + f_{i,j+1}^l\right),$$
$$i = P_{l-1}, \quad j = \overline{0,(N-1)}, \quad l = \overline{1,J}, \tag{26}$$

$$\frac{v_{i,j+1}^l - v_{i,j}^l}{\Delta t} = \frac{1}{2}\left(\frac{2c_l}{(\Delta x_l)^2}\bar{\delta}_x^2 u_{i,j}^l - d_l u_{i,j}^l + f_{i,j}^l + \frac{2c_l}{(\Delta x_l)^2}\bar{\delta}_x^2 u_{i,j+1}^l - d_l u_{i,j+1}^l + f_{i,j+1}^l\right),$$
$$i = P_l, \quad j = \overline{0,(N-1)}, \quad l = \overline{1,(J-1)}, \tag{27}$$

where:

$$\delta_x^2 u_{i,j}^l = u_{i-1,j}^l - 2u_{i,j}^l + u_{i+1,j}^l, \quad \tilde{\delta}_x^2 u_{i,j}^l = u_{i+1,j}^l - u_{i,j}^l - \Delta x_l\left(u_{i,j}^l\right)_x,$$
$$\bar{\delta}_x^2 u_{i,j}^l = u_{i-1,j}^l - u_{i,j}^l + \Delta x_l\left(u_{i,j}^l\right)_x.$$

Equations (18), (23), (19) and (20) are discretised as:

$$u_{i,0}^l = \phi_l(x_i), \quad v_{i,0}^l = \psi_l(x_i) + b_l\phi_l(x_i), \quad i = \overline{P_{l-1}, P_l}, \quad l = \overline{1,J}, \tag{28}$$

6

$$u^l_{P_l,j} = u^{l+1}_{P_l,j}, \quad \gamma_l \left(u^l_{P_l,j}\right)_x = \left(u^{l+1}_{P_l,j}\right)_x, \qquad j = \overline{0, N}, \qquad l = \overline{1, (J-1)}, \tag{29}$$

$$u^1_{0,j} + \beta \left(u^1_{0,j}\right)_x = R(t_j), \quad u^J_{P_J,j} = 0, \qquad j = \overline{0, N}. \tag{30}$$

Solving (24) for $v^l_{i,j+1}$, we obtain:

$$v^l_{i,j+1} = \left(b_l + \frac{2}{\Delta t}\right) u^l_{i,j+1} + \left(b_l - \frac{2}{\Delta t}\right) u^l_{i,j} - v^l_{i,j}, \tag{31}$$

for $i = \overline{P_{l-1}, P_l}, j = \overline{0, (N-1)}, l = \overline{1, J}.$

Introducing (31) in (25), we obtain:

$$-A_l u^l_{i-1,j+1} + B_l u^l_{i,j+1} - A_l u^l_{i+1,j+1} = A_l u^l_{i-1,j} + C_l u^l_{i,j} + A_l u^l_{i+1,j} + 2v^l_{i,j}$$
$$+ \frac{\Delta t}{2}\left(f^l_{i,j} + f^l_{i,j+1}\right), \tag{32}$$

where $i = \overline{(P_{l-1} + 1), (P_l - 1)}, j = \overline{0, (N-1)}, l = \overline{1, J}, A_l = \dfrac{c_l \Delta t}{2(\Delta x_l)^2}, B_l = \left(\dfrac{2}{\Delta t} + b_l\right) + \dfrac{c_l \Delta t}{(\Delta x_l)^2} + \dfrac{d_l \Delta t}{2}$ and $C_l = \left(\dfrac{2}{\Delta t} - b_l\right) - \left(\dfrac{c_l \Delta t}{(\Delta x_l)^2} + \dfrac{d_l \Delta t}{2}\right).$

Similarly, introducing (31) in (26), we obtain:

$$2\Delta x_{l+1} A_{l+1} \left(u^{l+1}_{P_l,j+1}\right)_x + B_{l+1} u^{l+1}_{P_l,j+1} - 2A_{l+1} u^{l+1}_{P_l+1,j+1} = -2\Delta x_{l+1} A_{l+1} \left(u^{l+1}_{P_l,j}\right)_x + C_{l+1} u^{l+1}_{P_l,j}$$
$$+ 2A_{l+1} u^{l+1}_{P_l+1,j} + 2v^{l+1}_{P_l,j} + \frac{\Delta t}{2}\left(f^{l+1}_{P_l,j} + f^{l+1}_{P_l,j+1}\right), \tag{33}$$

for $j = \overline{0, (N-1)}, l = \overline{0, (J-1)}$, and in (27), we obtain:

$$-2A_l u^l_{P_l-1,j+1} + B_l u^l_{P_l,j+1} - 2\Delta x_l A_l \left(u^l_{P_l,j+1}\right)_x = 2A_l u^l_{P_l-1,j} + C_l u^l_{P_l,j} + 2\Delta x_l A_l \left(u^l_{P_l,j}\right)_x$$
$$+ 2v^l_{P_l,j} + \frac{\Delta t}{2}\left(f^l_{P_l,j} + f^l_{P_l,j+1}\right), \tag{34}$$

for $j = \overline{0, (N-1)}, l = \overline{1, (J-1)}$. From (30), the difference equation (33) for $l = 0$ becomes:

$$(B_1 - \lambda) u^1_{0,j+1} - 2A_1 u^1_{1,j+1} = (C_1 + \lambda) u^1_{0,j} + 2A_1 u^1_{1,j} + 2v^1_{0,j} + \frac{\Delta t}{2}\left(f^1_{0,j} + f^1_{0,j+1}\right)$$
$$- \lambda \left(R(t_j) + R(t_{j+1})\right), \tag{35}$$

where $\lambda = 2A_1 \Delta x_1 / \beta$. For $j = \overline{0, (N-1)}, l = \overline{1, (J-1)}$, multiplying equations (33) and (34) by $\bar{\eta}_l := \Delta x_l A_l$ and by $\tilde{\eta}_l := \gamma_l \Delta x_{l+1} A_{l+1}$, respectively, summing the resulting equations and then using the continuity conditions given by (29), we obtain:

$$-\tilde{A}_l u^l_{P_l-1,j+1} + \tilde{B}_l u^l_{P_l,j+1} - \bar{A}_{l+1} u^{l+1}_{P_l+1,j+1} = \tilde{A}_l u^l_{P_l-1,j} + \tilde{C}_l u^l_{P_l,j} + \bar{A}_{l+1} u^{l+1}_{P_l+1,j}$$
$$+ 2(\tilde{\eta}_l v^l_{P_l,j} + \bar{\eta}_l v^{l+1}_{P_l,j}) + \frac{\Delta t}{2}\left(\tilde{\eta}_l(f^l_{P_l,j} + f^l_{P_l,j+1}) + \bar{\eta}_l(f^{l+1}_{P_l,j} + f^{l+1}_{P_l,j+1})\right), \tag{36}$$

where $\tilde{A}_l = 2\tilde{\eta}_l A_l, \bar{A}_{l+1} = 2\bar{\eta}_l A_{l+1}, \tilde{B}_l = \tilde{\eta}_l B_l + \bar{\eta}_l B_{l+1}$ and $\tilde{C}_l = \tilde{\eta}_l C_l + \bar{\eta}_l C_{l+1}.$

At each time step $t_{j+1} = (j+1)\Delta t$ for $j = \overline{0, (N-1)}$, the difference equations given by (31), (32), (35) and (36) can be reformulated as an implicit FDM procedure of the form:

$$\tilde{L}\tilde{\boldsymbol{u}}_{j+1} = \tilde{E}\tilde{\boldsymbol{u}}_j + 2\tilde{\boldsymbol{v}}_j + \tilde{\boldsymbol{b}}^j, \tag{37}$$

$$\boldsymbol{v}_{j+1}^l = \left(b_l + \frac{2}{\Delta t}\right)\boldsymbol{u}_{j+1}^l + \left(b_l - \frac{2}{\Delta t}\right)\boldsymbol{u}_j^l - \boldsymbol{v}_j^l, \quad l = \overline{1,\mathrm{J}}, \tag{38}$$

where:

$$\boldsymbol{u}_j^l = (u_{P_{l-1},j}^l, \ldots, u_{P_l,j}^l)^{\mathrm{T}}, \qquad \boldsymbol{v}_j^l = (v_{P_{l-1},j}^l, \ldots, v_{P_l,j}^l)^{\mathrm{T}}, \qquad \tilde{\boldsymbol{u}}_j = (u_{0,j}^1, \ldots, u_{P_{\mathrm{J}}-1,j}^{\mathrm{J}})^{\mathrm{T}},$$

$$\tilde{\boldsymbol{v}}_j = (v_{0,j}^1, \ldots, \tilde{\eta}_1 v_{P_1,j}^1 + \bar{\eta}_1 v_{P_1,j}^2, v_{P_1+1,j}^2, \ldots, \tilde{\eta}_{\mathrm{J}-1} v_{P_{\mathrm{J}-1},j}^{\mathrm{J}-1} + \bar{\eta}_{\mathrm{J}-1} v_{P_{\mathrm{J}-1},j}^{\mathrm{J}}, v_{P_{\mathrm{J}-1}+1,j}^{\mathrm{J}}, \ldots, v_{P_{\mathrm{J}}-1,j}^{\mathrm{J}})^{\mathrm{T}},$$

$$\tilde{L} = \begin{pmatrix} B_1 - \lambda & -2A_1 & & & & & & & & \\ -A_1 & B_1 & -A_1 & & & & & & & \\ & \ddots & \ddots & \ddots & & & & & & \\ & & -\tilde{A}_1 & \tilde{B}_1 & -\bar{A}_2 & & & & & \\ & & & -A_2 & B_2 & -A_2 & & & & \\ & & & & \ddots & \ddots & \ddots & & & \\ & & & & & -\tilde{A}_{\mathrm{J}-1} & \tilde{B}_{\mathrm{J}-1} & -\bar{A}_{\mathrm{J}} & & \\ & & & & & & -A_{\mathrm{J}} & B_{\mathrm{J}} & -A_{\mathrm{J}} & \\ & & & & & & & \ddots & \ddots & \ddots \\ & & & & & & & & -A_{\mathrm{J}} & B_{\mathrm{J}} \end{pmatrix},$$

$$\tilde{E} = \begin{pmatrix} C_1 + \lambda & 2A_1 & & & & & & & & \\ A_1 & C_1 & A_1 & & & & & & & \\ & \ddots & \ddots & \ddots & & & & & & \\ & & \tilde{A}_1 & \tilde{C}_1 & \bar{A}_2 & & & & & \\ & & & A_2 & C_2 & A_2 & & & & \\ & & & & \ddots & \ddots & \ddots & & & \\ & & & & & \tilde{A}_{\mathrm{J}-1} & \tilde{C}_{\mathrm{J}-1} & \bar{A}_{\mathrm{J}} & & \\ & & & & & & A_{\mathrm{J}} & C_{\mathrm{J}} & A_{\mathrm{J}} & \\ & & & & & & & \ddots & \ddots & \ddots \\ & & & & & & & & A_{\mathrm{J}} & C_{\mathrm{J}} \end{pmatrix},$$

$$\tilde{\boldsymbol{b}}^j = \begin{pmatrix} \dfrac{\Delta t}{2}\left(f_{0,j}^1 + f_{0,j+1}^1\right) - \lambda\left(R(t_j) + R(t_{j+1})\right) \\ \dfrac{\Delta t}{2}\left(f_{1,j}^1 + f_{1,j+1}^1\right) \\ \vdots \\ \dfrac{\Delta t}{2}\left(\tilde{\eta}_1\left(f_{P_1,j}^1 + f_{P_1,j+1}^1\right) + \bar{\eta}_1\left(f_{P_1,j}^2 + f_{P_1,j+1}^2\right)\right) \\ \dfrac{\Delta t}{2}\left(f_{P_1+1,j}^2 + f_{P_1+1,j+1}^2\right) \\ \vdots \\ \dfrac{\Delta t}{2}\left(\tilde{\eta}_{\mathrm{J}-1}\left(f_{P_{\mathrm{J}-1},j}^{\mathrm{J}-1} + f_{P_{\mathrm{J}-1},j+1}^{\mathrm{J}-1}\right) + \bar{\eta}_{\mathrm{J}-1}\left(f_{P_{\mathrm{J}-1},j}^{\mathrm{J}} + f_{P_{\mathrm{J}-1},j+1}^{\mathrm{J}}\right)\right) \\ \dfrac{\Delta t}{2}\left(f_{P_{\mathrm{J}-1}+1,j}^{\mathrm{J}} + f_{P_{\mathrm{J}-1}+1,j+1}^{\mathrm{J}}\right) \\ \vdots \\ \dfrac{\Delta t}{2}\left(f_{P_{\mathrm{J}}-1,j}^{\mathrm{J}} + f_{P_{\mathrm{J}}-1,j+1}^{\mathrm{J}}\right) \end{pmatrix}.$$

The above FDM scheme is second-order accurate in both space and time in the L_∞-norm and is unconditionally stable, [31].

Depending on the organ that is imaged the stratified specimen may have J = 3 layers, [11], J = 4 layers, [1], or even J = 7 layers, [32], for the skin, thigh or eye, respectively.

In the next two subsections we investigate a triple- and a four-layer tissue.

3.1 Three-layered tissue

In this physical example, we consider a one-dimensional, three-layered (J = 3) human skin tissue subjected to a short-time laser irradiation of the form, [11],

$$Q_e^l(x,t) = \mu I_0 H(t_{\mathrm{p}} - t)e^{-\mu x}, \quad (x,t) \in [L_{l-1}, L_l] \times (0, t_{\mathrm{f}}], \quad l = \overline{1, J}, \tag{39}$$

where μ is the extinction coefficient of the tissue [m^{-1}], I_0 denotes the intensity of the laser [W/m^2], t_{p} represents the laser irradiation's duration [s] and $H(t)$ is the Heaviside step function, and, for simplicity, the heat generation due to metabolism is neglected, i.e. $Q_m^l = 0$ for $l = \overline{1, J}$. In computations, the Heaviside step function $H(t)$ is approximated via the hyperbolic tangent function as:

$$H(t_{\mathrm{p}} - t) \approx \frac{1}{2}\left[1 + \tanh\left(\frac{50\,(t_{\mathrm{p}} - t)}{t_{\mathrm{f}}}\right)\right], \quad t \in (0, t_{\mathrm{f}}]. \tag{40}$$

The thermo-physical properties of the tissue layers given in Table 1 are taken from Table III of Autrique and Lormel [11]. The values of the other parameters are taken from the same reference as: $C_b = 3.9962 \times 10^6$ Joule/(m^3 K), $T_0 = T_a = T_\infty = 306$ K, $h = 10$ W/(m^2 K), $\mu = 700$ m^{-1}, $I_0 = 130 \times 10^3$ W/m^2, $t_{\mathrm{p}} = 1$ s and $t_{\mathrm{f}} = 20$ s. Further, we take the relaxation time $\tau = 20$ s, which is characteristic to biological bodies, [33, 34].

Table 1: Thermo-physical properties of a three-layered tissue, [11]. Note that 1 W = 1 Joule/s and $L_0 = 0$.

	Epidermis $(L_1 - L_0)$	Dermis $(L_2 - L_1)$	Hypodermis $(L_3 - L_2)$	Unit
Thickness	6×10^{-4}	1.4×10^{-3}	2×10^{-3}	m
k	0.235	0.425	0.185	W/(m K)
C_{t}	3.96×10^6	3.65×10^6	2.80×10^6	Joule/(m^3 K)
w_b	0	9.6592×10^{-4}	0	s^{-1}

To validate the FDM described in Section 3, we solve the dimensionless model (11)-(14) using various discretisations $N = M^l \in \{20, 30, 40\}$ for $l = \overline{1, 3}$ with J = 3 and the above input, which, via (10) and (15), yields:

$$\begin{aligned} &a_1^1 = a_1^3 = 1, a_1^2 = 1.0212, a_2^1 = 7.4179 \times 10^{-2}, a_2^2 = 1.4555 \times 10^{-1}, a_2^3 = 8.2589 \times 10^{-2}, \\ &a_3^1 = a_3^3 = 0, a_3^2 = 0.0212, a_4^1 = 1.5019, a_4^2 = 1.6295, a_4^3 = 2.1242, a_5^1 = 0.5529, \\ &a_5^2 = 2.2973, a_6 = 5.875, \theta_\infty = 0, \mathrm{L}_0 = 0, \mathrm{L}_1 = 0.15, \mathrm{L}_2 = 0.5, \mathrm{L}_3 = 1, \\ &F^l \approx 0.5\,(1 + \tanh(2.5 - 50t))\,e^{-2.8x}, \quad (x,t) \in [\mathrm{L}_{l-1}, \mathrm{L}_l] \times (0, 1], \quad l = \overline{1, 3}. \end{aligned} \tag{41}$$

Figure 2 shows the dimensionless temperature at the tissue surface $x = \mathrm{L}_0 = 0$ and at the midpoint of the hypodermis layer. From this figure, it can be clearly seen that the numerical

solution is convergent as the mesh size is reduced. Although the external heating radiates according to the short-time laser aggression (39), the negative non-dimensional temperature in Figure 2 indicates, see (10) with $T_0 = T_\infty$, that the actual dimensional temperatures $T_1(0,t)$ and $T_3(0.003,t)$ are lower than the ambient temperature $T_\infty = 306$ K. This is due to the hyperbolic model of bio-heat transfer given by equation (1), in which the negativeness of the time derivative $\frac{\partial Q_e^l}{\partial t}(x,t)$ makes the free term in equation (11) act as a sink rather than a source if the relaxation time $\tau_l > 0$ is taken into account. This type of anomaly in the analysis of hyperbolic heat conduction was previously highlighted by [35].

In contrast, the external heating (42) that is considered in the next subsection acts like a source making the dimensionless temperature in Figure 3 positive.
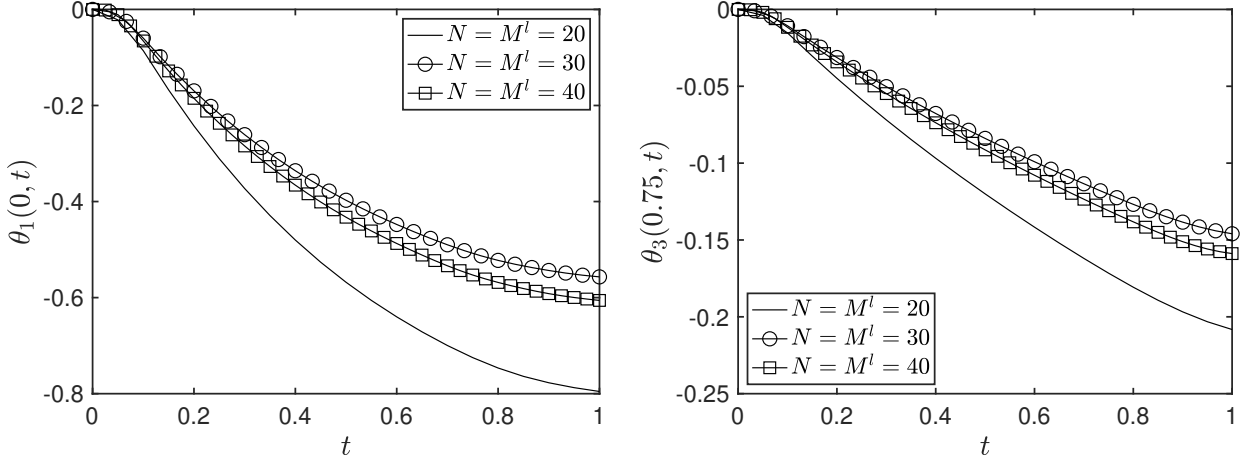
Figure 2: Numerical dimensionless temperatures $\theta_1(0,t)$ and $\theta_3(0.75,t)$, for various $N = M^l \in \{20,30,40\}$ for $l = \overline{1,3}$, for the direct problem of the three-layered tissue.

3.2 Four-layered tissue

In this physical example, we consider a one-dimensional, four-layered (skin, fat, muscles and bone) human thigh tissue subjected to an electromagnetic (EM) aggression of the form, [1],

$$Q_e^l(x,t) = \rho_t^l \kappa \Lambda_0 e^{g(x-0.01)}, \quad (x,t) \in [L_{l-1}, L_l] \times (0, t_f], \quad l = \overline{1,J}, \tag{42}$$

where κ [kg^{-1}] and g [m^{-1}] are constants of microwave antenna and Λ_0 is the EM aggression power [W]. For simplicity, the heat generation due to metabolism, Q_m^l for $l = \overline{1,4}$, has been neglected. The tissue's properties given in Table 2 are taken from Tunç et al. [1]. The values of the other parameters are taken from the same reference as: $C_b = 3.822 \times 10^6$ Joule/(m^3 °C), $T_0 = T_a = 37$ °C, $T_\infty = 20$ °C, $h = 10$ W/(m^2 °C), $\kappa = 12.5$ kg^{-1}, $g = -127$ m^{-1}, $\Lambda_0 = 20$ W and $t_f = 300$ s. Further, we take $\tau = 20$ s as before in the previous example.

To confirm the convergence of the FDM described in Section 3, we solve the dimensionless model (11)-(14) using various discretisations $N = M^l \in \{5,10,20\}$ for $l = \overline{1,4}$ with

Table 2: Thermo-physical properties of a four-layered tissue, [1].

	Skin $(L_1 - L_0)$	Fat $(L_2 - L_1)$	Muscle $(L_3 - L_2)$	Bone $(L_4 - L_3)$	Unit
Thickness	2.5×10^{-3}	10^{-2}	2.75×10^{-2}	10^{-2}	m
k	0.376	0.450	0.642	0.116	W/(m °C)
ρ_t	1000	850	1050	1500	kg/m³
c_t	3770	2300	3750	1590	Joule/(kg °C)
C_t	3.77×10^6	1.955×10^6	3.9375×10^6	2.385×10^6	Joule/(m³ °C)
w_b	9.3333×10^{-3}	6.0714×10^{-3}	2.6190×10^{-3}	0	s⁻¹

$J = 4$ and the above input, which, via (10) and (15), yields:

$$
\begin{aligned}
&a_1^1 = 17.8386, a_1^2 = 18.5609, a_1^3 = 15.7627, a_1^4 = 15, a_2^1 = 0.1795, a_2^2 = 0.4143, \\
&a_2^3 = 0.2935, a_2^4 = 0.0875, a_3^1 = 42.5793, a_3^2 = 53.413, a_3^3 = 11.44, a_3^4 = 0, a_4^1 = 28.7186, \\
&a_4^2 = 55.3806, a_4^3 = 27.4969, a_4^4 = 45.3959, a_5^1 = 0.8356, a_5^2 = 0.7009, a_5^3 = 5.5345, \\
&a_6 = 0.752, \theta_\infty = -0.4595, L_0 = 0, L_1 = 0.05, L_2 = 0.25, L_3 = 0.8, L_4 = 1, \\
&F^1 = 0.2808 e^{-6.35(x-0.2)}, F^2 = 0.2387 e^{-6.35(x-0.2)}, F^3 = 0.2949 e^{-6.35(x-0.2)}, \\
&F^4 = 0.4212 e^{-6.35(x-0.2)}.
\end{aligned}
\tag{43}
$$

Figure 3 depicts the dimensionless temperature at the tissue surface $x = L_0 = 0$ and at the midpoint of the muscle layer. From this figure, it can be clearly observed that the numerical solution is convergent as the mesh size is reduced.
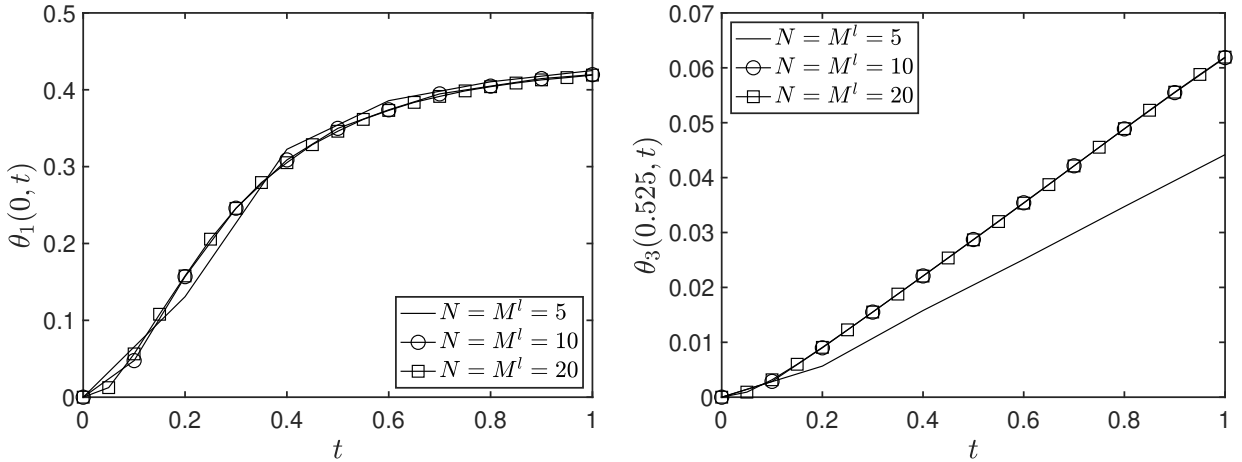

Figure 3: Numerical dimensionless temperatures $\theta_1(0, t)$ and $\theta_3(0.525, t)$, for various $N = M^l \in \{5, 10, 20\}$ for $l = \overline{1, 4}$, for the direct problem of the four-layered tissue.

The next section presents a numerical optimisation approach used for the inversion of the thermo-physical parameters, after which two inverse problems, associated with the direct problems of Section 3, are solved.

4. Numerical approach to solve the inverse problem

For notational convenience, in what follows, we denote the solution of the direct problem (11)-(14) by $\theta(x, t)$, which is piecewise equal to θ_l over the lth-layer for $l = \overline{1, J}$. The inverse

problem considered is that of reconstructing the physical parameters $\left(k_l, C_{\mathrm{t}}^l, w_b^l\right)_{l=\overline{1,\mathrm{J}}}$ of the dimensional model (5)-(9) from point-wise observations of the tissue temperature supplied at the distinct internal points ξ^n for $n = \overline{1,\mathrm{I}}$. These internal temperature measurements are numerically simulated prior to inversion by solving the direct problem (11)-(14) using the FDM solver described in Section 3 with $N = M^l = 640$ for $l = \overline{1,\mathrm{J}}$. Afterwards, the inverse problem is solved with a coarser mesh of $N_{\mathrm{inv}} = M_{\mathrm{inv}}^l = 320$ for $l = \overline{1,\mathrm{J}}$, which is different from the previous mesh in order to avoid committing an inverse crime. Furthermore, to mimic practical measurements in which errors are inherently present, random noise is added to the numerically simulated data as:

$$\theta^\epsilon(\xi^n, t_j) = \theta(\xi^n, t_j) + \epsilon_j^n, \quad j = \overline{1, N_{\mathrm{inv}}}, \quad n = \overline{1,\mathrm{I}}, \tag{44}$$

where ϵ_j^n are random variables generated from a Gaussian normal distribution with zero mean and standard deviations σ_n given by:

$$\sigma_n = p \times \max_{j=\overline{1,N_{\mathrm{inv}}}} |\theta(\xi^n, t_j)|, \quad n = \overline{1,\mathrm{I}}, \tag{45}$$

where p denotes the percentage of noise. The MATLAB command $normrnd(0, \sigma_n, N_{\mathrm{inv}})$ is employed to produce the random variables $\left(\epsilon_j^n\right)_{j=\overline{1,N_{\mathrm{inv}}}}$ for $n = \overline{1,\mathrm{I}}$.

Therefore, in the inversion below, we attempt to recover the vector $\boldsymbol{a} := \left(a_1^l, a_2^l, a_4^l\right)_{l=\overline{1,\mathrm{J}}}$ of the dimensionless model (11)-(14) by minimising the least-squares objective function defined by:

$$G(\boldsymbol{a}) = \sum_{n=1}^{\mathrm{I}} \sum_{j=1}^{N_{\mathrm{inv}}} \left[\theta(\xi^n, t_j) - \theta^c(\xi^n, t_j; \boldsymbol{a})\right]^2, \tag{46}$$

where $\theta^c(\xi^n, t_j; \boldsymbol{a})$ for $n = \overline{1,\mathrm{I}}$ stand for the computed temperatures at each iteration of the minimisation procedure. In the case of noisy measurements, $\theta(\xi^n, t_j)$ for $n = \overline{1,\mathrm{I}}$ are replaced by $\theta^\epsilon(\xi^n, t_j)$ (defined in (44)) in (46).

To this end, we invoke the MATLAB *lsqnonlin* subroutine which attempts to find the minimum of a sum of squares subject to simple physical constraints on the unknowns by starting from an arbitrary initial guess, [36]. We prescribe the lower and upper bounds for $\left(a_1^l\right)_{l=\overline{1,\mathrm{J}}}$ to be t_{f}/τ and 10^3, respectively, and for $\left(a_2^l\right)_{l=\overline{1,\mathrm{J}}}$ and $\left(a_4^l\right)_{l=\overline{1,\mathrm{J}}}$ to be 10^{-3} and 10^3, respectively. The initial guess for $\left(a_1^l\right)_{l=\overline{1,\mathrm{J}}}$ is taken to be $1.5t_{\mathrm{f}}/\tau$, and for $\left(a_2^l\right)_{l=\overline{1,\mathrm{J}}}$ and $\left(a_4^l\right)_{l=\overline{1,\mathrm{J}}}$ to be 0.5, which are reasonably far from their true values given in (41) or (43). Other parameters associated with the built-in MATLAB *lsqnonlin* subroutine are specified as follows:

- Algorithm is the Trust-Region-Reflective (TRR) minimisation, [37].

- Maximum number of iterations = 150.

- Maximum number of objective function evaluations = $10^3 \times$ (number of variables).

- Termination tolerance on the function value = 10^{-20}.

- Solution tolerance = 10^{-20}.

To examine the accuracy of the identified parameters, the relative error (RE%) is used, as defined by:

$$\text{RE}(\zeta) = \frac{|\zeta^{\text{numerical}} - \zeta^{\text{exact}}|}{|\zeta^{\text{exact}}|} \times 100\%, \tag{47}$$

where $\zeta^{\text{numerical}}$ stands for the numerical value obtained and ζ^{exact} denotes the exact value of the parameter of interest, if available.

4.1 Three-layered tissue

In this first example, we solve the inverse problem of reconstructing the physical parameters $\left(k_l, C_{\text{t}}^l, w_b^l\right)_{l=\overline{1,3}}$ of the dimensional model (5)-(9) for the three-layered tissue considered in Section 3.1 from measurements of the tissue temperature at ξ^n for $n = \overline{1, \text{I}}$. For the present inverse problem, we assume that the temperature measurements are taken at the tissue surface $x = L_0 = 0$ and at the midpoints of the epidermis, dermis and hypodermis layers (the dimensionless positions of the measurements are 0, 0.075, 0.325 and 0.75, respectively). Precisely, we investigate I = 1 ($\xi^1 = 0$), I = 2 ($\xi^1 = 0$ and $\xi^2 = 0.75$), I = 3 ($\xi^1 = 0$, $\xi^2 = 0.325$ and $\xi^3 = 0.75$) and I = 4 ($\xi^1 = 0$, $\xi^2 = 0.075$, $\xi^3 = 0.325$ and $\xi^4 = 0.75$) point-wise observations.

We first consider noiseless data, i.e. $p = 0$ in (45), and run the MATLAB built-in *lsqnonlin* subroutine for I $\in \{1, 2, 3, 4\}$ point-wise observations. Figure 4 depicts the convergence of the objective function G defined in (46), as a function of the number of iterations, for I $\in \{1, 2, 3, 4\}$ point-wise observations. From this figure, it can be concluded that the objective function G attains lower minimal values when considering I = 3 measurements compared to the cases I $\in \{1, 2\}$. Moreover, the behaviour of the objective function G is similar when I = 3 or I = 4. We thus choose the solution found for I = 3, as the desired physical solution. We next consider $p = 0.1\%$ noise in (45) with I = 3 and employ the MATLAB built-in *lsqnonlin* subroutine. Figure 4 shows the convergence of the objective function G, as a function of the number of iterations, for this case of noisy data.
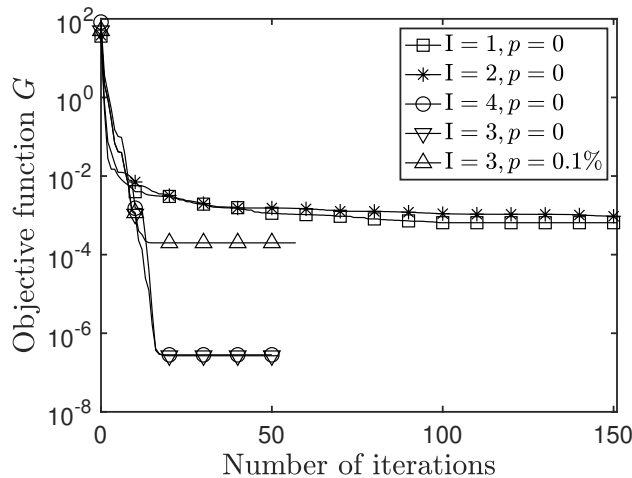
Figure 4: The objective function G defined in (46), as a function of the number of iterations, for I $\in \{1, 2, 4\}$ and $p = 0$, and for I = 3 and $p \in \{0, 0.1\%\}$ noise, for the inverse problem of the three-layered tissue.

Tables 3 and 4 show the reconstructed values of the dimensionless parameters $\left(a_1^l, a_2^l, a_4^l\right)_{l=\overline{1,3}}$ for I $\in \{1, 2, 4\}$ and $p = 0$, and for I = 3 and $p \in \{0, 0.1\%\}$ noise, respectively. Additional

details regarding the minimisation of the objective function (46), such as its values at the identified solutions, the number of iterations and the elapsed time are also included in Table 4. The values of the dimensional constant parameters $\left(k_l, C_t^l, w_b^l\right)_{l=\overline{1,3}}$ of the thermal-wave model given by equations (5)-(9) can be found from the formulae given by equation (16), and they are presented in Table 5. Clearly, from Table 3 it can be seen that the numerically retrieved values of the coefficients are far from their true values for I $\in \{1, 2\}$. This indicates that not enough information has been supplied in order to retrieve uniquely the unknown coefficients. Consequently, the number of measurements has been increased to I $= 3$ and 4 and accurate reconstructions for the unknowns can be observed from Tables 3-5 in case of errorless measured temperature data with $p = 0$. Furthermore, reconstructions are also shown to be stable when inverting data contaminated with $p = 0.1\%$ noise, as can be seen from Tables 4 and 5. Note that since the blood perfusion rates w_b^l for $l = \overline{1, 3}$ are $\mathcal{O}(10^{-4})$ small, the use of the absolute error instead of the relative error might be more appropriate in order to interpret and discuss the very good accuracy and stability in the numerical reconstructions presented in Table 5.

Table 3: Identified values of $\left(a_1^l, a_2^l, a_4^l\right)_{l=\overline{1,3}}$ when I $\in \{1, 2, 4\}$ and $p = 0$, for the inverse problem of the three-layered tissue.

	Exact	I = 1		I = 2		I = 4	
		Identified	RE (%)	Identified	RE (%)	Identified	RE (%)
a_1^1	1	1.0002	0.02	1.0000	5×10^{-5}	1.0000	4×10^{-12}
a_1^2	1.0212	1.0003	2.04	1.1920	16.73	1.0212	9×10^{-4}
a_1^3	1	6.8242	582.4	1.0000	2×10^{-12}	1.0000	4×10^{-12}
a_2^1	7.4179×10^{-2}	10.725	14359	6.3706	8488	0.0742	0.01
a_2^2	1.4555×10^{-1}	0.7207	395.2	0.0667	54.15	0.1455	7×10^{-5}
a_2^3	8.2589×10^{-2}	1.1544	1298	0.0823	0.34	0.0827	0.12
a_4^1	1.5019	1.7051	13.52	1.7983	19.73	1.5020	5.8×10^{-3}
a_4^2	1.6295	2.4642	51.22	1.5429	5.31	1.6296	5.1×10^{-3}
a_4^3	2.1242	9.8169	362.2	2.1247	0.02	2.1243	6.3×10^{-3}
G		6.48×10^{-4}		9.43×10^{-4}		2.82×10^{-7}	

4.2 Four-layered tissue

In this second example, we solve the inverse problem of identifying the physical parameters $\left(k_l, C_t^l, w_b^l\right)_{l=\overline{1,4}}$ of the dimensional model (5)-(9) for the four-layered tissue considered in Section 3.2 from measurements of the tissue temperature at ξ^n for $n = \overline{1, I}$. For the current inverse problem, we assume that the temperature measurements are supplied at the tissue surface $x = L_0 = 0$ and at the midpoints of the fat, muscle and bone layers (the dimensionless positions of the measurements are 0, 0.15, 0.525 and 0.9, respectively). Precisely, we investigate I $= 1$ ($\xi^1 = 0$), I $= 2$ ($\xi^1 = 0$ and $\xi^2 = 0.9$), I $= 3$ ($\xi^1 = 0$, $\xi^2 = 0.525$ and $\xi^3 = 0.9$) and I $= 4$ ($\xi^1 = 0$, $\xi^2 = 0.15$, $\xi^3 = 0.525$ and $\xi^4 = 0.9$) point-wise observations.

We first consider noiseless data, i.e. $p = 0$ in (45), and invoke the MATLAB built-in *lsqnonlin* subroutine for I $\in \{1, 2, 3, 4\}$ point-wise observations. Figure 5 displays the convergence of the objective function G, as a function of the number of iterations, for I $\in \{1, 2, 3, 4\}$ point-wise observations. From this figure, it can be seen that the objective function (46) attains lower minimal values when considering I $= 4$ measurements compared to the other

Table 4: Identified values of $\left(a_1^l, a_2^l, a_4^l\right)_{l=\overline{1,3}}$ and the relative errors (RE%), when I = 3 and $p \in \{0, 0.1\%\}$ noise, for the inverse problem of the three-layered tissue.

		$p = 0$		$p = 0.1\%$	
	Exact	Identified	RE (%)	Identified	RE (%)
a_1^1	1	1.0000	4×10^{-12}	1.0007	6.7×10^{-2}
a_1^2	1.0212	1.0212	2.6×10^{-3}	1.0199	1.2×10^{-1}
a_1^3	1	1.0000	4×10^{-10}	1.0000	9.4×10^{-4}
a_2^1	7.4179×10^{-2}	7.4204×10^{-2}	3.3×10^{-2}	7.3761×10^{-2}	5.6×10^{-1}
a_2^2	1.4555×10^{-1}	1.4550×10^{-1}	3.6×10^{-2}	1.4599×10^{-1}	3.0×10^{-1}
a_2^3	8.2589×10^{-2}	8.2692×10^{-2}	1.2×10^{-1}	8.2729×10^{-2}	1.7×10^{-1}
a_4^1	1.5019	1.5021	7.5×10^{-3}	1.5015	2.9×10^{-2}
a_4^2	1.6295	1.6296	6.8×10^{-3}	1.6289	3.9×10^{-2}
a_4^3	2.1242	2.1243	6.2×10^{-3}	2.1245	1.3×10^{-2}
G		2.67×10^{-7}		1.99×10^{-4}	
Number of iterations		52		57	
Elapsed time		16 s		18 s	
Reason of halting iteration		Norm of current step is less than step tolerance, 10^{-20}			

Table 5: Identified values of $\left(k_l, C_t^l, w_b^l\right)_{l=\overline{1,3}}$ and the relative errors (RE%), when I = 3 and $p \in \{0, 0.1\%\}$ noise, for the inverse problem of the three-layered tissue.

		$p = 0$		$p = 0.1\%$	
	Exact	Identified	RE (%)	Identified	RE (%)
k_1	0.235	0.2351	2.5×10^{-2}	0.2337	5.3×10^{-1}
k_2	0.425	0.4248	4.3×10^{-2}	0.4265	3.4×10^{-1}
k_3	0.185	0.1852	1.2×10^{-1}	0.1853	1.6×10^{-1}
C_t^1	3.96×10^6	3.9597×10^6	7.5×10^{-3}	3.9611×10^6	2.9×10^{-2}
C_t^2	3.65×10^6	3.6498×10^6	6.8×10^{-3}	3.6514×10^6	3.9×10^{-2}
C_t^3	2.80×10^6	2.7998×10^6	6.2×10^{-3}	2.7996×10^6	1.3×10^{-2}
w_b^1	0	2.1782×10^{-15}	—	3.3393×10^{-5}	—
w_b^2	9.6592×10^{-4}	9.6707×10^{-4}	1.2×10^{-1}	9.0981×10^{-4}	5.81
w_b^3	0	1.4708×10^{-13}	—	3.2906×10^{-7}	—

three cases. We therefore choose the solution found for I = 4, as the desired physical solution. We next consider $p = 0.1\%$ noise in (45) with I = 4 and run the MATLAB built-in *lsqnonlin* subroutine. Figure 5 presents the convergence of the objective function G, as a function of the number of iterations, for this case of noisy data.

Tables 6 and 7 show the identified values of the dimensionless parameters $\left(a_1^l, a_2^l, a_4^l\right)_{l=\overline{1,4}}$ for $I \in \{1, 2, 3\}$ and $p = 0$, and for I = 4 and $p \in \{0, 0.1\%\}$ noise, respectively. Additional details regarding the minimisation of the objective function (46), such as its values at the reconstructed solutions, the number of iterations and the elapsed time are also included in Table 7. The values of the dimensional constant parameters $\left(k_l, C_t^l, w_b^l\right)_{l=\overline{1,4}}$ of the thermal-wave model given by equations (5)-(9) can be found from the formulae given by equation (16),
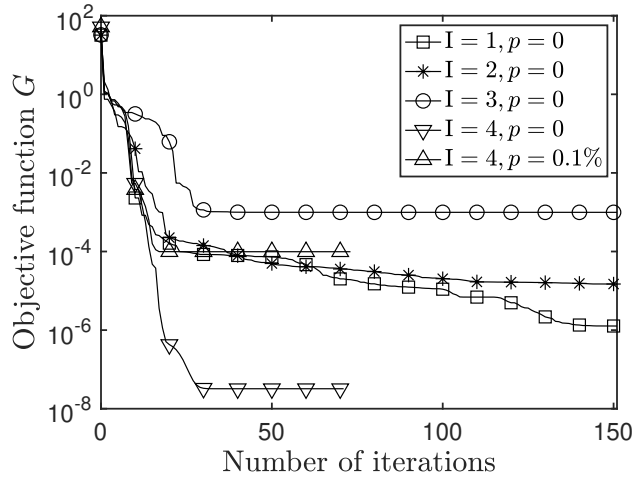
Figure 5: The objective function G defined in (46), as a function of the number of iterations, for $I \in \{1, 2, 3\}$ and $p = 0$, and for $I = 4$ and $p \in \{0, 0.1\%\}$ noise, for the inverse problem of the four-layered tissue.

and they are presented in Table 8. Clearly, from the rather poor numerical reconstructions presented in Table 6 it can be seen that $I = 1, 2$ or 3 internal temperature measurements are not sufficient to retrieve all the 12 unknowns of the four-layered tissue. On the other hand, the numerical reconstructions obtained with $I = 4$ internal temperature measurements presented in Tables 7 and 8 illustrate an accurate and stable retrieval of the unknown parameters. Note that since the blood perfusion rates w_b^l for $l = \overline{1, 4}$ are $\mathcal{O}(10^{-3})$ small, the use of the absolute error instead of the relative error might be more appropriate in order to interpret and discuss the very good accuracy and stability in the numerical reconstructions presented in Table 8.

Table 6: Identified values of $\left(a_1^l, a_2^l, a_4^l\right)_{l=\overline{1,4}}$ when $I \in \{1, 2, 3\}$ and $p = 0$, for the inverse problem of the four-layered tissue.

		I = 1		I = 2		I = 3	
	Exact	Identified	RE (%)	Identified	RE (%)	Identified	RE (%)
a_1^1	17.8386	17.8945	0.31	18.5914	4.22	20.0789	12.5
a_1^2	18.5609	18.8974	1.81	17.1831	7.42	16.5779	10.7
a_1^3	15.7627	20.5417	30.3	20.0015	26.9	16.6426	5.58
a_1^4	15.0000	22.5000	50.0	15.3986	2.66	15.4054	2.70
a_2^1	0.1795	0.1786	0.53	0.1574	12.3	266.275	10^5
a_2^2	0.4143	0.3360	18.9	38.0517	10^4	0.2191	47.1
a_2^3	0.2935	0.0010	99.6	0.5208	77.5	0.5799	97.6
a_2^4	0.0875	0.5000	471.1	0.0429	50.9	0.0360	58.9
a_4^1	28.7186	28.8213	0.36	30.0590	4.67	24.3111	15.3
a_4^2	55.3806	56.9625	2.86	88.5900	59.9	372.949	573.4
a_4^3	27.4969	58.3760	112.3	71.0670	158.4	29.3131	6.60
a_4^4	45.3959	0.5000	98.9	48.3672	6.54	48.7687	7.43
G		1.27×10^{-6}		1.49×10^{-5}		9.93×10^{-4}	

16

Table 7: Identified values of $\left(a_1^l, a_2^l, a_4^l\right)_{l=\overline{1,4}}$ and the relative errors (RE%), when I = 4 and $p \in \{0, 0.1\%\}$ noise, for the inverse problem of the four-layered tissue.

		$p = 0$		$p = 0.1\%$	
	Exact	Identified	RE (%)	Identified	RE (%)
a_1^1	17.8386	17.8383	1.8×10^{-3}	17.8266	6.7×10^{-2}
a_1^2	18.5609	18.5608	5.7×10^{-4}	18.5639	1.6×10^{-2}
a_1^3	15.7627	15.7630	2.3×10^{-3}	15.7708	5.2×10^{-2}
a_1^4	15.0000	15.0000	5×10^{-10}	15.0041	2.8×10^{-2}
a_2^1	0.1795	0.1798	1.7×10^{-1}	0.1813	9.9×10^{-1}
a_2^2	0.4143	0.4145	3.3×10^{-2}	0.4213	1.69
a_2^3	0.2935	0.2936	5.1×10^{-2}	0.2969	1.16
a_2^4	0.0875	0.0876	4.9×10^{-3}	0.0866	1.11
a_4^1	28.7186	28.7139	1.6×10^{-2}	28.6558	2.2×10^{-1}
a_4^2	55.3806	55.3821	2.6×10^{-3}	55.4605	1.4×10^{-1}
a_4^3	27.4969	27.4972	9.2×10^{-4}	27.4994	9.0×10^{-3}
a_4^4	45.3959	45.3963	9.4×10^{-4}	45.4006	1.0×10^{-2}
G		3.22×10^{-8}		9.88×10^{-5}	
Number of iterations		71		73	
Elapsed time		69 s		71 s	
Reason of halting iteration		Norm of current step is less than step tolerance, 10^{-20}			

Table 8: Identified values of $\left(k_l, C_t^l, w_b^l\right)_{l=\overline{1,4}}$ and the relative errors (RE%), when I = 4 and $p \in \{0, 0.1\%\}$ noise, for the inverse problem of the four-layered tissue.

		$p = 0$		$p = 0.1\%$	
	Exact	Identified	RE (%)	Identified	RE (%)
k_1	0.376	0.3767	1.8×10^{-1}	0.3806	1.21
k_2	0.450	0.4501	3.0×10^{-2}	0.4570	1.55
k_3	0.642	0.6423	4.9×10^{-2}	0.6494	1.15
k_4	0.116	0.1160	3.9×10^{-3}	0.1147	1.12
C_t^1	3.77×10^6	3.7706×10^6	1.6×10^{-2}	3.7783×10^6	2.2×10^{-1}
C_t^2	1.955×10^6	1.9549×10^6	2.6×10^{-3}	1.9522×10^6	1.4×10^{-1}
C_t^3	3.9375×10^6	3.9375×10^6	9.2×10^{-4}	3.9371×10^6	9.0×10^{-3}
C_t^4	2.385×10^6	2.3850×10^6	9.4×10^{-4}	2.3847×10^6	1.0×10^{-2}
w_b^1	9.3333×10^{-3}	9.3338×10^{-3}	4.9×10^{-3}	9.3143×10^{-3}	2.0×10^{-1}
w_b^2	6.0714×10^{-3}	6.0711×10^{-3}	5.6×10^{-3}	6.0679×10^{-3}	5.9×10^{-2}
w_b^3	2.6190×10^{-3}	2.6203×10^{-3}	4.7×10^{-2}	2.6468×10^{-3}	1.06
w_b^4	0	1.6823×10^{-13}	—	8.6130×10^{-6}	—

5. Conclusions

The thermal-wave model of bioheat transfer in multi-layered biological tissues has been considered. An iterative numerical procedure based on the MATLAB built-in *lsqnonlin* subroutine has been proposed and successfully applied for the simultaneous reconstruction of the

17

thermo-physical properties of multi-layered biological tissues. Numerical results associated with two physical examples concerning one-dimensional, three- and four-layered tissues have been presented and thoroughly discussed. It has been found, as shown in Tables 5 and 8, that the accuracy and stability of the numerical results for the simultaneous reconstructions of the thermo-physical properties $\left(k_l, C_{\mathrm{t}}^l, w_b^l\right)_{l=\overline{1,\mathrm{J}}}$ of the thermal-wave model given by equations (5)-(9) are possible if sufficient internal temperature data is measured.

Future work will consist in the determination of the thermo-physical properties of multi-layered biological tissues in the more general third-order dual-phase-lag model of bio-heat transfer, [8].

References

[1] M. Tunç, Ü. Çamdali, C. Parmaksizoğlu, S. Çikrikçi, The bio-heat transfer equation and its applications in hyperthermia treatments, Eng. Comput. 23 (4) (2006) 451–463.

[2] M. Baghban, M.B. Ayani, Source term prediction in a multilayer tissue during hyperthermia, J. Therm. Biol. 52 (2015) 187–191.

[3] H.H. Pennes, Analysis of tissue and arterial blood temperatures in the resting human forearm, J. Appl. Physiol. 1 (2) (1948) 93–122.

[4] V.P. Peshkov, Second sound in helium II, Sov. Phys. JETP 11 (3) (1960) 580–584.

[5] B. Bertman, D.J. Sandiford, Second sound in solid helium, Sci. Am. 222 (5) (1970) 92–101.

[6] K. Mitra, S. Kumar, A. Vedavarz, M.K. Moallemi, Experimental evidence of hyperbolic heat conduction in processed meat, J. Heat Transf.-Trans. ASME 117 (3) (1995) 568–573.

[7] J. Liu, Z. Ren, C. Wang, Interpretation of living tissue's temperature oscillations by thermal wave theory, Chin. Sci. Bull. 40 (17) (1995) 1493–1495.

[8] J.-R. Ho, Ch.-P. Kuo, W.-S. Jiaung, Study of heat transfer in multilayered structure within the framework of dual-phase-lag heat conduction model using lattice Boltzmann method, Int. J. Heat Mass Transf. 46 (1) (2003) 55–69.

[9] E. Majchrzak, G. Kałuża, Analysis of thermal processes occurring in heated multilayered metal films using the dual-phase lag model, Arch. Mech. 69 (4-5) (2017) 275–287.

[10] E. Majchrzak, B. Mochnacki, Dual-phase lag model of thermal processes in a multi-layered microdomain subjected to a strong laser pulse using the implicit scheme of FDM, Int. J. Therm. Sci. 133 (2018) 240–251.

[11] L. Autrique, C. Lormel, Numerical design of experiment for sensitivity analysis–application to skin burn injury prediction, IEEE Trans. Biomed. Eng. 55 (4) (2008) 1279–1290.

[12] K. Yue, X. Zhang, Y.Y. Zuo, Noninvasive method for simultaneously measuring the thermophysical properties and blood perfusion in cylindrically shaped living tissues, Cell Biochem. Biophys. 50 (2008) 41–51.

[13] S. Panda, R. Das, A golden section search method for the identification of skin subsurface abnormalities, Inverse Probl. Sci. Eng. 26 (2) (2018) 183–202.

[14] K. Das, S.C. Mishra, Estimation of tumor characteristics in a breast tissue with known skin surface temperature, J. Therm. Biol. 38 (6) (2013) 311–317.

[15] H.-L. Lee, T.-H. Lai, W.-L. Chen, Y.-C. Yang, An inverse hyperbolic heat conduction problem in estimating surface heat flux of a living skin tissue, Appl. Math. Model. 37 (5) (2013) 2630–2643.

[16] M. Rojczyk, H.R.B. Orlande, M.J. Colaço, I. Szczygieł, A.J. Nowak, R.A. Białecki, Z. Ostrowski, Inverse heat transfer problems: an application to bioheat transfer, Comput. Assist. Meth. Eng. Sci. 22 (4) (2015) 365–383.

[17] P.W. Partridge, L.C. Wrobel, An inverse geometry problem for the localisation of skin tumours by thermal analysis, Eng. Anal. Bound. Elem. 31 (10) (2007) 803–811.

[18] J. Iljaž, L.C. Wrobel, M. Hriberšek, J. Marn, Numerical modelling of skin tumour tissue with temperature-dependent properties for dynamic thermography, Comput. Biol. Med. 112 (2019) pp. 103367.

[19] S. Panda, R. Das, Parameter estimation in a biological system using differential evolution algorithm, 2018 Eleventh International Conference on Contemporary Computing (IC3), IEEE, Noida, 2018, pp. 18263042.

[20] M. Alosaimi, D. Lesnic, J. Niesen, Reconstruction of the thermal properties in a wave-type model of bio-heat transfer, Int. J. Numer. Methods Heat Fluid Flow 30 (12) (2020) 5143–5167.

[21] S.R. Edmondson, S.P. Thumiger, G.A. Werther, C.J. Wraight, Epidermal homeostasis: the role of the growth hormone and insulin-like growth factor systems, Endocr. Rev. 24 (6) (2003) 737–764.

[22] K.-C. Liu, P.-J. Cheng, Finite propagation of heat transfer in a multilayer tissue, J. Thermophys. Heat Transf. 22 (4) (2008) 775–782.

[23] Y.J. Yu, Analytical solutions to hyperbolic heat conductive models using Green's function method, J. Therm. Sci. Technol. 13 (1) (2018) pp. JTST0012.

[24] M.J. Maurer, H.A. Thompson, Non-Fourier effects at high heat flux, J. Heat Transf.-Trans. ASME 95 (2) (1973) 284–286.

[25] D. Jou, V.A. Cimmelli, A. Sellitto, Nonequilibrium temperatures and second-sound propagation along nanowires and thin layers, Phys. Lett. A 373 (47) (2009) 4386–4392.

[26] V.A. Cimmelli, D. Jou, A. Sellitto, Propagation of temperature waves along core-shell nanowires, J. Non-Equilib. Thermodyn. 35 (2010) 267–278.

[27] M.G. Hennessy, M. Calvo-Schwarzwälder, T.G. Myers, Modelling ultra-fast nanoparticle melting with the Maxwell–Cattaneo equation, Appl. Math. Model. 69 (2019) 201–222.

[28] J. Liu, X. Chen, L.X. Xu, New thermal wave aspects on burn evaluation of skin subjected to instantaneous heating, IEEE Trans. Biomed. Eng. 46 (4) (1999) 420–428.

[29] M. Alosaimi, D. Lesnic, J. Niesen, Identification of the thermo-physical properties of a stratified tissue. Adiabatic hypodermic wall, Int. Commun. Heat Mass Transf. (2021). Submitted for publication.

[30] W. Dai, R. Nassar, A finite difference scheme for solving the heat transport equation at the microscale, Numer. Meth. Part Differ. Equ. 15 (6) (1999) 697–708.

[31] H. Sun, Z.-Z. Sun, W. Dai, A second-order finite difference scheme for solving the dual-phase-lagging equation in a double-layered nanoscale thin film, Numer. Meth. Part Differ. Equ. 33 (1) (2017) 142–173.

[32] A. Narasimhan, S. Sadasivam, Non-Fourier bio heat transfer modelling of thermal damage during retinal laser irradiation, Int. J. Heat Mass Transf. 60 (2013) 591–597.

[33] W. Kaminski, Hyperbolic heat conduction equation for materials with a nonhomogeneous inner structure, J. Heat Transf.-Trans. ASME 112 (3) (1990) 555–560.

[34] Ş. Özen, S. Helhel, O. Çerezci, Heat analysis of biological tissue exposed to microwave by using thermal wave model of bio-heat transfer (TWMBT), Burns 34 (1) (2008) 45–49.

[35] A. Haji-Sheikh, W.J. Minkowycz, E.M. Sparrow, Certain anomalies in the analysis of hyperbolic heat conduction, J. Heat Transf.-Trans. ASME 124 (2) (2002) 307–319.

[36] Mathworks, Documentation optimization toolbox-least squares (model fitting) algorithms, (2012). available at: www.mathworks.com/help/toolbox/optim/ug/brnoybu.html.

[37] T.F. Coleman, Y. Li, An interior trust region approach for nonlinear minimization subject to bounds, SIAM J. Optim. 6 (2) (1996) 418–445.